DOI: 10.1002/ejic.200900550

Two Self-Catenated Nickel(II) Hybrid Vanadates with Honeycomb-Like 3D Inorganic Frameworks Stabilized by Crossed Organic Bpe Pillars: Thermal, Spectroscopic and Magnetic Properties

Roberto Fernández de Luis,[a] Jose L. Mesa,*[b] M. Karmele Urtiaga,[a] Teófilo Rojo,[b] and María Isabel Arriortua[a]

Keywords: Crystal engineering / Hybrid materials / Vanadates / Hydrothermal synthesis / Magnetic properties

The three-dimensional hybrid compounds $[\{Ni_6(H_2O)_{10}(Bpy)_6\}V_{18}O_{51}]\cdot 1.5H_2O$ (**1**, Bpy = 4,4′-bipyridine) and $[\{Ni(H_2O)_2(Bpe)\}V_4O_{11}]\cdot 0.5H_2O$ (**2**, Bpe = 1,2-bis(4-pyridyl)ethene) have been synthesized under mild hydrothermal conditions. The 3D crystal structures of both compounds are closely related, with an inorganic honeycomb-like framework stabilized by the organic ligands. The latter are oriented in a crossed way into the channel of the inorganic backbone, and directly attached to the nickel(II) metal centers. Increasing of the ligand length causes widening of the inorganic skeleton with retention of the main structural organization. Both compounds possess self-catenated nets, a 24-nodes net $(3\text{-c})_2(4\text{-c})_3(5\text{-c})_7$ for **1** and a binodal net (4-c)(7-c) for **2**. These rigid architectures exhibit very interesting thermal properties. The co-crystallized water molecules can be removed without changes in the crystal structures. The initial phases show a low thermal expansion of the cell volume, with a negative thermal expansion of the *b* parameter for compound **1**. Moreover, at high temperatures structural irreversible transformations are observed in both compounds, due to the removal of coordinated water molecules. These transformations have been followed by thermodiffractometry and IR spectra. The UV/Vis spectra show the characteristic bands of the Ni^{II} d^8-high spin cation in slightly distorted octahedral environment. The magnetic behaviour is strongly dependent of the connectivity of the metal centres through the VO_5 polyhedra. Compound **1** exhibits a typical Zero Field Splitting for six nickel(II) cations, while the shortest distances between the nickel(II) ions in **2** allow a weak antiferromagnetic 1D coupling.

Introduction

The construction of new inorganic-organic hybrid compounds through the rational combination of organic ligands ("spacers"), metal nodes and different anions has become an area of great interest recently due to the potential application in catalysis, hydrogen storage, molecular adsorption, electromagnetism and photochemistry. Although hybrid materials are expected to exhibit improved properties and functions not seen in pure inorganic or organic phases,[1] studies on thermal properties are still rare. The flexibility of the organic part of the crystal structures, combined with a rigid inorganic framework could give rise to near-zero or negative thermal expansion.

The synergetic interaction between the organic and inorganic components allows a partial degree of crystal engineering by exploiting fundamental aspects of the structural organization: (i) coordination preferences and oxidation states of the metal centres. (ii) The length of the spacer, geometry, degree of flexibility and relative position of the ligand donor groups. (iii) The structural influence of the anion on the framework organization and assembly adopted by the different metal-organic moieties.[2]

In concrete terms, hybrid vanadates with first-row transition metal centres exhibit very rich crystal chemistry, with several structural archetypes in function of the metal centre, geometry of the ligand and the vanadium oxide subunit. Owing to the ability of vanadium to adopt a variety of coordination environments in various oxidation states, recent interest has focused on their potential use as secondary cathode materials for advanced lithium batteries,[3] their importance in industrial oxidative catalysis[4] and photocatalytic activity.[5]

From this point of view, the combination of dipodal ligands like, pyrazine, 4,4′-bipyridine or 1,2-bis(4-pyridyl)-ethene, with first-row transition metal centers, and the vanadate oxoanion gives rise to several 3D inorganic-organic

[a] Departamento de Mineralogía y Petrología, Facultad de Ciencia y Tecnología, Universidad del País Vasco/EHU, Apdo. 644, 48080 Bilbao, Spain
[b] Departamento de Química Inorgánica, Facultad de Ciencia y Tecnología, Universidad del País Vasco/EHU, Apdo. 644, 48080 Bilbao, Spain
Fax: +34-946013500
E-mail: joseluis.mesa@ehu.es
Supporting information for this article is available on the WWW under http://dx.doi.org/10.1002/ejic.200900550.

architectures. These polytopic organic amino ligands serve to bond the metal sites and to propagate the structural information express in the metal coordination preferences through the extended structure.[6] The expansive chemistry of coordination polymers bound to pyrazine, 4,4′-bipyridine and 1,2-bis(4-pyridyl)ethene includes one-, two- and three-dimensional metal-organic subnets exhibiting diamond, grid, ladder, brick, railroad and octahedral building blocks.[7] Usually, the combination of the metal-organic subnet and the vanadium oxide subunit gives rise to crystal structures constructed from inorganic layers pillared by the organic ligand.[8] Such materials are still rare, their three-dimensional architectures exhibit a 3D inorganic framework stabilized by organic molecules.[9–10]

Modification of the hydrothermal synthesis conditions, such as time, temperature, stoichometry, pH, concentration[11] and filling factor, allows partial control of the oxoanion polimerization degree giving rise to different $\{V_xO_y\}$ species that are stable in solution.[12] Examples of are the $\{V_2O_7\}$ dimers, $\{V_4O_{12}\}$ cyclic tetramers or $\{VO_3\}$ metavanadate chains. Recently, we reported the effect of the initial concentration and pH value in the hydrothermal synthesis of the Ni/Bpy/V_xO_y and Ni/Bpe/V_xO_y systems.[13] In this respect, high concentrations and acidic conditions promote five-coordinated vanadium, more polymerized $\{V_xO_y\}$ subunits, and hence more condensed three-dimensional inorganic frameworks stabilized with metal–ligand chains. Interestingly, the crystal structures obtained under neutral or slightly acidic conditions contain four-coordinated vanadium, more complex metal-organic moieties, and less condensated inorganic architectures.

In this work we describe the mild hydrothermal synthesis of two inorganic-organic hybrid compounds, $[\{Ni_6(H_2O)_{10}(Bpy)_6\}V_{18}O_{51}]\cdot 1.5H_2O$ (**1**) and $[\{Ni(H_2O)_2(Bpe)\}V_4O_{11}]\cdot 0.5H_2O$ (**2**), their thermal behaviour, spectroscopic and magnetic properties. Moreover, the topological analysis of the compounds reveals self-catenated entanglements. The vanadium oxide subunit promotes the formation of highly linked frameworks, and hence favoures the self-catenation phenomenon.[14] Of the many reported types of entanglements[15] the phenomenon of self-catenation has attracted much attention in recent times. Until now, only a few have been observed in metal-organic frameworks.

Results and Discussion

Crystal Structures

The crystal structures of $[\{Ni_6(H_2O)_{10}(Bpy)_6\}V_{18}O_{51}]\cdot 1.5H_2O$ (**1**) (see part a of Figure 1) and $[\{Ni(H_2O)_2(Bpe)\}V_4O_{11}]\cdot 0.5H_2O$ (**2**) (Figure 2, a) are an example of a rigid 3D inorganic honeycomb-like framework stabilized by bidentate organic ligands like 4,4′-bipyridine or 1,2-bis(4-pyridyl)ethene, respectively.

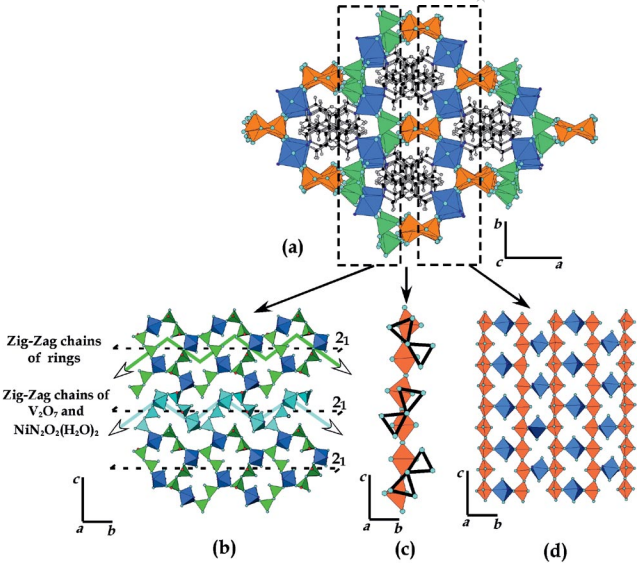

Figure 1. a) Three dimensional crystal structures of **1**. (b) Connectivity between V_2O_7 dimers and nickel octehedra. (c) Connectivity between the metavanadate chains and the V_2O_7 subunits. (d) Connectivity between the metavanadate chains and nickel octahedra.

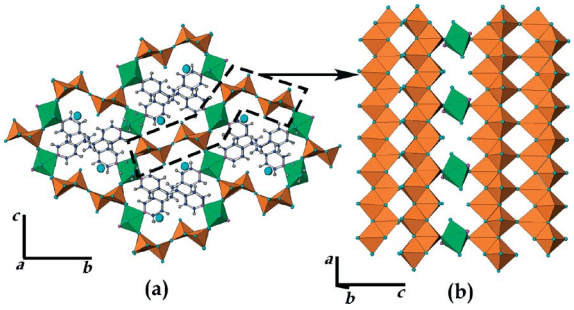

Figure 2. (a) Crystal structure of **2**. (b) Connectivity between the double metavanadate chains and the $NiN_2O_2(H_2O)_2$ octahedra.

The chiral phase **1** crystallizes in the monoclinic space group $P2_1$. The high volume of the unit cell and the low symmetry of the space group generate 209 crystallographic independent atoms. The crystal structure is constructed from four different structural subunits: i) V_2O_7 dimers of corner-linked VO_4 tetrahedra, ii) metavanadate chains of edge-shared VO_5 polyhedra, iii) two types of nickel(II) octahedra $NiN_2O_2(H_2O)_2$, and $NiN_2O_3H_2O$, and iv) the bpe organic ligand (Figure 1). The crystal structure possesses three crystallographically independent V_2O_7 subunits with different orientations (Figure 1, b and c). The connectivity between the dimers and the octahedra generates layers constructed from two kind of helical chains (Figure 1, b). The $NiN_2O_3(H_2O)$ octahedra links three V_2O_7 subunits giving rise to zig-zag chains of nine polyhedra rings (Figure 1, b). The $NiN_2O_2(H_2O)_2$ octahedra are corner-shared by two V_2O_7 subunits generating helical chains (Figure 1, b). Both chains are corner-linked and give rise to an unprecedented connectivity.

The metavanadate chains consist of twelve edge-shared crystallographically independent VO_5 polyhedra. This subunit has two kinds of linkages, one of its sides is linked to the V_2O_7 dimers (Figure 1, c), and the other one is shared with the $NiN_2O_2(H_2O)_2$ octahedra (Figure 1, d). The connectivity between the vanadium oxide subunits and the nickel(II) octahedra generates a honeycomb-like inorganic framework.

The organic ligand is directly attached to the Ni^{II} metal centers and exhibits a crossed disposition in the channels of the crystal structure. The co-crystallized water molecules are encapsulated between the crossed Bpy molecules and the inorganic three-dimensional framework.

The metavanadate-chains or the V_2O_7 dimers have been previously reported for different hybrid vanadates, but the presence of both structural subunits in the same crystal structure is sufficiently distinct from those of the other metal oxides and it has not precedent in the literature. Moreover, the orientation of the V_2O_7 subunits brokes the centre of symmetry giving rise to the chirality in the final framework.

The crystal structure of **2** is an example of an expanded inorganic honeycomb-like inorganic framework due to the increase of the ligand length (Figure 2, a). The unit cell contains one $NiN_2O_2(H_2O)_2$ octahedra, four VO_5 polyhedra, and one Bpe molecule. The vanadium oxide subunit is constructed from two corner-linked matevanadate chains of edge-shared VO_5 polyhedra, giving rise to a double metavanadate chain (Figure 1, b) The vanadium oxide subunit is disordered in two positions with 0.5 occupation factor (see Figure S.1 in the Supporting Information).

Each double vanadate chain is connected to nickel octahedra in four different directions (Figure 2), generating a three-dimensional honeycomb-like inorganic framework. The nickel(II) octahedral environment is completed with two-coordinate water molecules and two nitrogen atoms. The ligands are linked to the Ni^{II} cations, and pointing to the centre of the inorganic channels. The orientation of the Bpe molecules generates a crossed disposition of the organic ligand in crystal structure. The co-crystallized water molecules are encapsulated between the crossed Bpe molecules and the inorganic framework.

The topological analysis of the crystal structures gives rise to two self-catenated nets. The topology of **1** consists of 24 nodal net with point symbol $\{3^3.4^2.5.7.8^3\}_4$ $\{3^3.4^2.5.7^2.8^2\}$ $\{3^3.4^2.5.8^3.9\}$ $\{3^3.4^3.5^2.6.7\}_2$ $\{3^3.4^3.5^3.6\}_4$ $\{4.5.7^2.8^2\}_2$ $\{4.5.7\}_2$ $\{4.7.8\}$ $\{4.8^2\}$ $\{5.7^2.8^6.12\}$ $\{5.7^3.8^5.12\}$ $\{7.8^4.10\}$ $\{7.8^4.12\}$ $\{7^2.8^3.10\}_2$ (Figure 3, a). The complexity of the net is related with the different connectivities between the vanadium oxide subunits, nickel octahedra and Bpy ligand. Parts (b) and (c) of Figure 3 depict the simplification of the vanadate chains and dimers and its connectivity with the nickel atoms. For **2** the net is a binodal (4-c)(7-c) connected self-catenated net with point symbol $\{3^6.4^4.6^9.7^2\}\{6^5.10\}$ (Figure 3, d). The vanadate chains and its simplification are shown in parts e and f of Figure 3. The vanadium nodes are seven-connected, and are linked to five vanadium nodes, related with the vanadate chains, and two nickel ones. The nickel nodes are four connected, and links to two nickel ones through the Bpe ligand, and two vanadium nodes of the metavanadate chains. The highly connected V_xO_y sub-

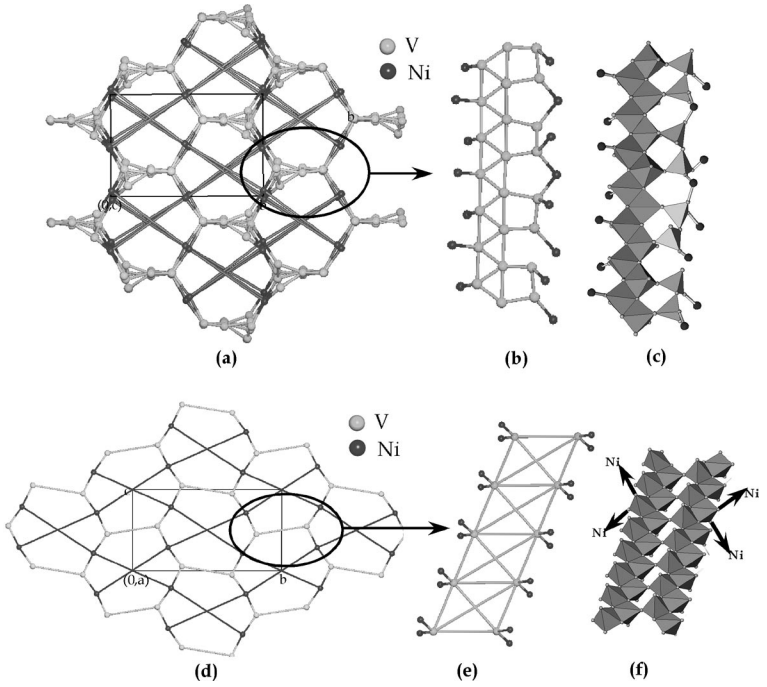

Figure 3. (a) 24-Nodal self-catenated net of **1**. (b) Simplification of the vanadium oxide subunit and the connectivity with the nickel atoms. (c) Vanadium oxide subunit and its connectivity with the nickel cations. (d) Binodal self-catenated net for 2. (e) Vanadate chains simplification. (f) Vanadate chains.

units of **1** and **2** promote the self-catenation entanglements, and increase the complexity of the obtained topologies.[16]

The bond lengths for **1** and **2** are depicted in the Figures S.2 and S.3 (see Supporting Information). The Ni–O and Ni–N bond lengths are in good agreement with slightly distorted octahedral environments, ranging from 2.02–2.16 Å (for **1**) and 2.04–2.10 Å (for **2**). The V–O bond lengths are strongly dependent on the oxygen atom connectivity. From this point of view, the shorter V–O bonds are related with the terminal oxygen atoms and these ones corner-linked to the nickel(II) cation. The V–O bonds with the oxygen atom shared by VO_5 and/or VO_4 polyhedra possess slightly longer distances.[17] The bond valance calculations for compounds **1** and **2** are resumed in the Table 1, and are in good agreement with 5+ and 2+ oxidation state for the vanadium(V) and nickel(II) ions, respectively.[18]

Table 1. Bond balance for the nickel and vanadium atoms in **1** and **2**.

Phase (1)				Phase (2)	
Ni(1)	2.006	V(7)	5.113	Ni	2.121
Ni(2)	2.062	V(8)	5.141	V(1)A	5.212
Ni(3)	2.053	V(9)	5.108	V(1)B	5.048
Ni(4)	1.973	V(10)	5.042	V(2)A	5.130
Ni(5)	2.020	V(11)	5.091	V(2)B	5.112
Ni(6)	1.987	V(12)	5.175	V(3)A	5.215
V(1)	5.145	V(13)	5.038	V(3)B	5.100
V(2)	5.108	V(14)	5.095	V(4)A	5.285
V(3)	5.146	V(15)	4.980	V(4)B	5.169
V(4)	5.175	V(16)	4.928		
V(5)	5.054	V(17)	5.008		
V(6)	5.041	V(18)	4.950		

Thermal Behaviour

The TGA and ATD curves for the studied compounds (Figure S.4) exhibit a continuous weight loss of 2.2% (for **1**) and 2.9% (for **2**) between room temperature and 180 °C. These values are higher than those calculated for the removal of co-crystallized water, 0.84% (for **1**) and 1.35% (for **2**), indicating that the process is overlapped with the loss of adsorbed water.

The loss of co-crystallized water molecules in these materials finished at high temperatures. This is not surprising because these ones are encapsulated between the organic ligands and the inorganic framework. The TGA and DTA curves of **1** show that the thermal decomposition is initiated by the loss of coordinated water molecules. The observed weight loss (5.4%) in the 180–280 °C temperature range corresponds to the release of ten water molecules per formula unit (calcd. 5.58%). The DTA curve, between 180 and 280 °C exhibits a continuous plateau, suggesting that the removal of coordinated water molecules is a continuous process during the whole temperature range. Furthermore, the weight loss (29.7%) occurring at 370–480 °C is related to the calcination of six bipyridine molecules per formula unit (calcd. 29.01%). A similar thermal behaviour is observed for **2**, with a initial weight loss of 5.8% in the temperature range 200–290 °C related to the removal of coordination water molecules (calcd. 5.41%). The DTA curve shows broad maxima, suggesting that the process occurs during the whole temperature range (200–290 °C). A second weight loss (27.6%), is observed at 370–450 °C, corresponding to the calcination of one Bpe molecule per formula unit (calcd. 27.37%).

The thermal stability of **1** and **2** was also studied by time-resolved X-ray thermodiffractometry in air (Figure S.5). Phase **1** is stable up to 260 °C, but the crystallinity decreases dramatically by 210 °C. At this temperature, a second compound starts to crystallize but disappears at 430 °C (Figure S.5, a). The thermogravimetric study shows the loss of coordinated water molecules between 210–280 °C. Taking this fact into account, the loss of coordinated water molecules gives rise to a strong reorganization of the crystal structure, promoting the crystallization of the anhydrous phase up to 210 °C. Moreover, the crystallinity is drastically reduced during the transformation, hindering the study of the anhydrous phase by X-ray diffraction. This one is stable up to 430 °C, but the patterns show an appreciable decrease of the intensity upon 380 °C. At higher temperatures several inorganic vanadates and vanadium oxides are observed: NiV_3O_8 (410–470 °C) → NiV_2O_6 + V_2O_5 (470–750 °C) → $Ni_2V_2O_7$. The thermodiffractometry of **2** reveals that the initial phase retains its crystal structure in the 30–260 °C temperature range, but the intensity of the diffraction maxima shows an appreciable reduction up to 210 °C. The anhydrous phase began to crystallize at 210 °C, and coexists with the hydrated one between 210 and 260 °C, disappearing at 400 °C. After the calcination of the organic molecule, the $Ni_2V_2O_7$ and V_2O_5 inorganic phases crystallize.

In the same way as for compound **1**, a drastic reduction of the crystallinity is observed during the transformation process of **2**. For this phase the position of the diffraction maxima in the hydrated compound can be related to the position of these corresponding to the anhydrous phase. Taking into account that the crystal structure of the anhydrous compound probably is related to the initial one, the unit cell has to be similar. However, the intensity of the reflections changes drastically during the removal of coordination water molecules (Figure S.6, a). The position of the (020) reflection is displaced from 7.9 to 7.4° in 2θ while the (011) maximum changes its position from 8.3 to 9.0°. The pattern maching refinement of the anhydrous phase was carried out with the Fullproff program.[19]

The initial values of the *b* and *c* parameters were calculated from the position of (020) and (110) reflections. The obtained cell parameters (Table 2) have to be considered

Table 2. Cell parameter for the initial phase **2** and the anhydrous one.

	a [Å]	*b* [Å]	*c* [Å]	*β* [°]
Phase **2**	7.2721(3)	23.062(2)	12.4826(6)	91.245(4)
Anhydrous **2**	7.722(9)	24.18(1)	10.824(3)	91.3(1)

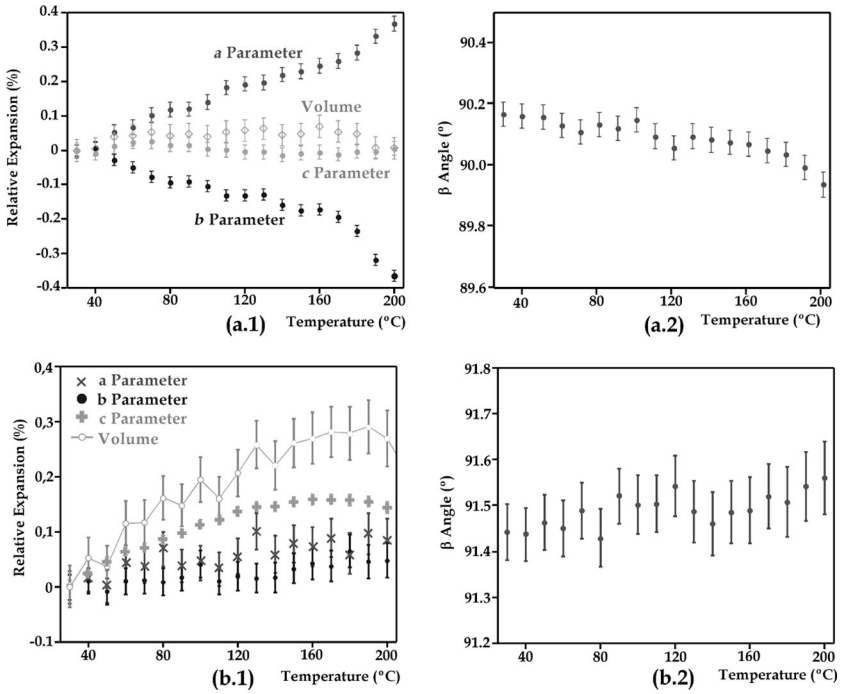

Figure 4. Thermal evolution of the cell parameter and the β angle. (a.1)–(a.2) compound **1**. (b.1)–(b.2) compound **2**.

qualitatively, because the pattern of the anhydrous phase exhibits poor crystallinity, with only few and broad maxima in the measured 2θ range.

The removal of coordination water molecules is probably compensated by the generation of new Ni–O bonds with the terminal oxygen atoms of the VO_5 polyhedra (Figure S.6, b). This connectivity shortens the distances between the adjacent vanadate chains, and hence reduces the *c* parameter. The same connectivity between the nickel(II) ions and the vanadate chains is observed in the inorganic vanadate $Ni(VO_3)_2{\cdot}4H_2O$.[20] The cooperative movements of the structural subunits imply a strong reorganization of the crystal structure, and hence promote a reduction of the crystal domains, diminishing the crystallinity of the patterns.

An interesting feature of the initial phases **1** and **2** is that the diffraction maxima don not show a strong displacement during the heating process before the transformation. The cyclic Rietveld refinement of the crystal parameters with respect to the temperature describes the thermal expansion of the crystal structures. Owing to the preferred orientation of the samples there are problems in the fit of some reflection intensities. However, the introduction of a fixed structural model allows us a better description of the thermal behaviour. The relative expansion of the crystal parameters has been calculated using the following equation: R.E. (%) $= [(P_T/P_{T(0)}) - 1] \times 100$, where P_T and $P_{T(0)}$ are the parameter values at the studied temperatures, and $T = 30$ °C, respectively. The thermal evolution of the cell parameters and the cell volume are shown in part a.1 of Figure 4 for **1** and in part b.1 for **2**.

The crystal structure of **1** shows a near zero thermal expansion of the volume in the temperature range 30–200 °C. The thermal evolution of the cell parameters shows a negative thermal expansion of the *b* parameter (–0.4%), and the increase of the *a* parameter (+0.4%). During the heating process the *c* parameter remains practically unchanged and the β angle shows a slight decrease of its value. The thermal behaviour of compound **2** is different in comparison with that corresponding to **1**, despite the similarities of the crystal structures. The *a* and *b* parameters slightly increase their values. The *c* parameter shows a relative expansion of 0.13% between room temperature and 130 °C, and at higher temperatures the expansion is blocked and retains its value approximately constant. The β angle remains approximately unchanged during the heating process. The thermal behaviour of the volume is strongly correlated to *c*.

The crystal structures of **1** and **2** do not seem to be influenced by the removal of crystal water molecules. This is not surprising if we take into account the rigid three-dimensional inorganic frameworks stabilised by the organic ligand of the crystal structure.

For **1** the crossed disposition of the Bpy molecules in the inorganic pseudo-hexagonal channels restricts the thermal expansion of the *a* and *b* parameters. If the *a* parameter presents a positive expansion, the *b* parameter has to show a decrease of its value, to keep the Ni···Ni distance approximately constant. Hence, these opposite trends cancel the contribution of both parameters, and the thermal behaviour of the volume is closely related to the slight thermal expansion of *c*.[21] The compound **2** also possess a crossed disposition of the Bpe ligand in the channels of the inorganic framework. However, the Bpe ligand is slightly inclined in the channels direction. This fact could promote the thermal expansion of *c*, until the process is blocked at higher temperatures.

UV/Vis and IR Spectroscopy

In the diffuse reflectance spectrum, two absorption bands of strong intensity corresponding to the allowed transitions: $^3A_{2g}(^3F) \rightarrow {}^3T_{2g}(^3F)$, $^3T_{1g}(^3F)$, at 9200, and 15400 cm^{-1} for **1**, and 9500 and 15660 for **2**, and the forbidden one $^3A_{2g}(^3F) \rightarrow {}^1E_{1g}(D)$ at 13100 cm^{-1} for **1** and 13300 cm^{-1} for **2**, are observed. From the spin transitions corresponding to the d^8-high spin Ni^{II} cation in octahedral geometry, the *Dq* and Racah *B* and *C* parameters have been calculated, by using the energy expressions given in the Tanabe–Sugano diagrams.[22] The values for compound **1** are $Dq = 940$, $B = 930$ cm^{-1} and $C = 3350$ cm^{-1}, and those ones for compound **2** are $Dq = 950$, $B = 955$ and $C = 3120$ cm^{-1}. The value of the *B* parameter is approximately 90% of that of the free Ni^{II} cation (1030 cm^{-1}), which indicates an appreciable covalent character in the chemical bonds inside the octahedron. The *Dq* and *B* values indicate a weak crystal field, and are in good agreement with those previously reported for compounds with slightly distorted octahedral environment.

The IR spectra were collected from a pristine sample (see Figure S.7 in the Supporting Information), then after heating at different temperatures during one hour. The evolutions of the more representative absorption maxima for compound **1** are depicted in the Figure S.8. The same ones for compound **2** are shown in Figure S.9. The changes of the IR spectra for **1** and **2** are very similar.

For **2**, the progressive reduction of the band related to the stretching vibration of the O–H bonds (Figure S.9, a) is in good agreement with the loss of crystallization (25–125 °C) and elimination of the coordinated (175–250 °C) water molecules. The removal of co-crystallized water molecules do not modify the bands related with the organic molecule (Figure S.9, b) and vanadium oxide subunit (Figure S.9, c and d).[23] This fact is in good agreement with the thermodiffractometric study.

After the removal of coordinated water molecules, the vibrational stretching C=C band is split in two signals (Figure S.9, b), and the absorption maxima related to the breathing of the pyridyl rings are broadening (Figure S.9, c). However, the most important differences in the IR spectra are related to the vibrational modes of the vanadium oxide subunit (Figure, S.9, c and d). Concretely, the position and intensity of the bands related with the V=O and V–O–V stretching vibrations (Figure S.9, c) which changes drastically during the transformation process.

Similar changes are observed in the infrared spectra of **1**, but here the coordinated water molecules do not disappear up to 250 °C. The IR spectra of the sample heated at this temperature shows a drastic change in the intensity and the position of the band associated to the vanadium oxide, and minor change in the bands associated to the vibrations of the Bpy molecule (Figure S.8).

In both compounds, the changes of the IR spectra suggest a strong reorganization of the vanadium oxide subunit and minor changes in the organic molecules during the removal of coordinated water molecules.

Magnetic Behaviour

The temperature susceptibilities of **1** and **2** have been measured in the range 300–5 K. The $\chi_m T$ values at 300 K per nickel(II) atom are, 1.462 cm^3 K/mol for **1**, and 1.645 cm^3 K/mol for **2**. These ones are higher than the expected for an isolated $S = 1$ ion ($\chi_m T = 1.21$ cm^3 K mol g = 2.2), due to the contribution from the temperature independent magnetism.

The χ_m vs. temperature curve for compound **1** shows a continuous increasing of its value between 300–5 K (Figure 5). Due to the large distance between Ni^{II} ions (approx. 6.2, 7.3 and 11.2 Å through the VO_4 tetrahedra, VO_5 polyhedra and Bpy ligand, respectively) significant exchange interactions between the metal centres are not expected. Therefore, the decreasing of the $\chi_m T$ value with decreasing temperature is attributed to the Zero Field Splittting, typical for an axially distorted d^8 high spin isolated Ni^{II} system. Considering an additional χ_{TIP} to account the temperature independent paramagnetism. The best fitting parameters obtained (solid line in Figure 5, a) are $D/hc = -14.4(2)$ cm^{-1}, $g = 2.199(1)$ and $\chi_{TIP} = 0.0051(5)$ cm^3 mol^{-1}. The *D* parameter value is consistent with the observed slightly distorted octahedral coordination environment for Ni^{II} cations,[24] and still well within the generally observed rather broad range from –22 to +12 cm^{-1}.

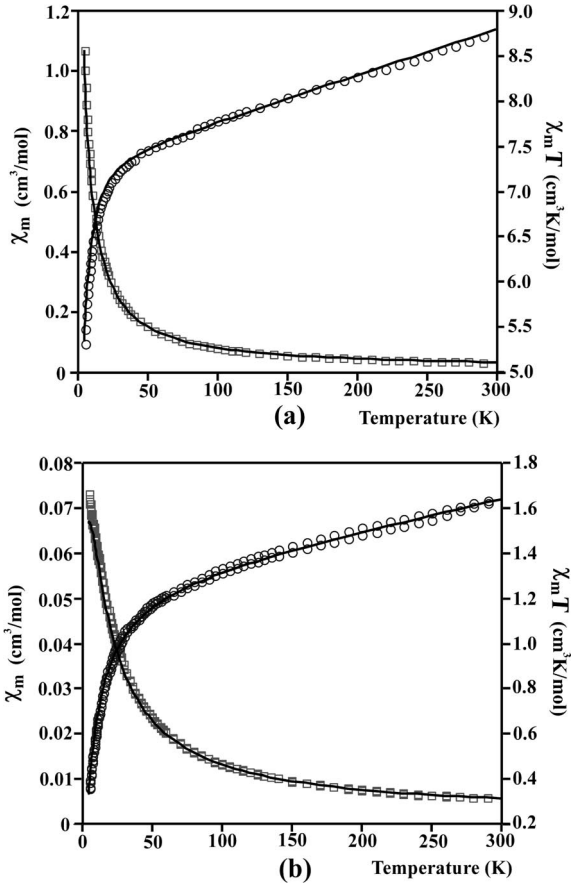

Figure 5. Plot of χ_m (circles) and $\chi_m T$ (squares) vs. temperature, (a) for **1**, (b) for **2**.

The thermal evolutions of the molar magnetic susceptibility, χ_m, and $\chi_m T$ vs. T curves for **2** are shown in Figure 5 (b). The molar susceptibility increases from 300 to 5 K. In the same way that in compound **1**, due to the large distance between the nickel(II) cations, 6.26 Å through the VO_5 polyhedra, a strong magnetic coupling is not expected. The χ_m and $\chi_m T$ curves were fitted considering the same model used in compound **1**, but the poor fit of the data, and the D/hc = 37(4) cm^{-1} value, out of the usually observed ones between –22 to 12 cm^{-1}, suggest a weak antiferromagnetic exchange between the metal centres. As the shortest distance Ni···Ni across the Bpy ligand is 13.63 Å, the overall antiferromagnetic interaction should be mainly attributed to the superexchange coupling within the inorganic framework. The Ni···Ni distance through the VO_5 polyhedra along the [010] direction is 6.26 Å, and the connectivity between the metal centres across the O–V–O atoms suggest the existence of one-dimensional magnetic behaviour [Figure S.10 (Supporting Information)]. The distance between adjacent chains in the crystal structure is 12.11 Å, very large for an interchain magnetic coupling. The magnetic data were thus analyzed according to an isotropic chain model[25] for S = 1 ions, and taking into account the temperature-independent paramagnetism. The theoretical fitting resulted in parameter g = 2.27(2), J/k = –5.80(4) and χ_{TIP} = 0.00127(6) emu/mol (Figure 5, b, solid line).

Conclusions

Two inorganic-organic nickel(II) vanadates with a 3D inorganic framework stabilized by bipodal ligands have been hydrothermally synthesized. Their crystal structures possess a similar organization of the vanadium oxide subunits, nickel(II) octahedra and organic ligands, giving rise to an expansion of the inorganic honeycomb like inorganic framework, due to the increase of the length of the organic ligand. The topological analysis gives rise to self-catenated nets for both compounds. This type of entanglement is promoted by the highly connected vanadium oxide subunits. The strong frameworks give rise to low thermal expansion of the initial phases, without any appreciable change in the crystal structure due to the removal of co-crystallized water molecules. Moreover, at higher temperatures the loss of coordinated water molecules generates an irreversible structural transformation with an important decrease in crystallinity. IR spectroscopy suggests an important structural reorganization of the vanadium oxide subunit during the transformation. The magnetic behaviour is strongly dependent of the metal center connectivity, and phase 1 exhibits a typical zero-field splitting for the nickel(II) ions, while phase 2 shows a 1D antiferromagnetic coupling due to the link of the nickel(II) cations through the VO_5 polyhedra.

Experimental Section

General: Commercially available chemicals (reagent grade) were purchased from Sigma–Aldrich, without further purifications. All synthetic reactions were carried out in Teflon®-lined 50 mL Parr acid digestion bombs.

Synthesis of $[\{Ni_6(H_2O)_{10}(Bpy)_6\}(V_{18}O_{51})]\cdot 1.5H_2O$ (1): A mixture consisting of $NaVO_3$ (0.78 mmol), 4,4′-bipyridine (0.26 mmol), $Ni(NO_3)_2\cdot 6H_2O$ (0.26 mmol), and H_2O (30 mL) in the molar ratio 1:3:1 was placed in a 50-mL Teflon®-lined Parr autoclave. The initial pH value was adjusted to 4.0 with a 1 M HNO_3 solution. After the mixture was stirred for 1 min, the autoclave was sealed and heated for 3 d in an electric furnace maintained at 170 °C. After the reaction time yellow prismatic single crystals of **1** with a very small amount of an unidentified yellow microcrystalline phase were obtained. The entire sample was dispersed in ca. 30 mL of water and sonicated for 10 min. The water was poured off after allowing the single crystals to settle for 20 min. This process was repeated until a pure sample of **1** was obtained, as judged by PXRD and visually under a microscope.

$[\{Ni(H_2O)_2(Bpe)\}(V_4O_{11})]\cdot 0.5H_2O$ (2): A mixture consisting of $NaVO_3$ (0.78 mmol), 1,2-bis(4-pyridyl)ethylene (0.135 mmol), $Ni(NO_3)_2\cdot 6H_2O$ (0.135 mmol), and H_2O (30 mL) in the molar ratio 1:6:1 was placed in a 50-mL Teflon®-lined Parr autoclave. The initial pH value was adjusted to 4.0 with 1 M HNO_3 under a vigorous stirring. The autoclave was sealed and heated for 3 d at 120 °C. A mixture of orange single crystals of **2** and green single crystals of previously reported $\{Ni(Bpe)\}(VO_3)_2$ was obtained.[26] The orange single crystals of **2** were mechanically separated from the green crystals. All attempts to obtain **2** as a single phase after the hydrothermal reaction were unsuccessful.

The synthesized samples were characterized by X-ray powder diffraction data. The patterns were recorded by means of a PHILIPS X'PERT diffractometer (Cu-K_α radiation) for **1** (2θ range: 5–90°, step size: 0.02°, time exposure: 5 s per step), and in a Bruker Advance Vario diffractometer (Cu-K_α radiation) for 2 (2θ range: 5–70°, step size: 0.015°, time exposure: 10 s per step). The Rietveld refinement with a fixed structural model, confirm the inexistence of impurities, despite problems in the fit of some reflections intensity due to the preferred orientation of the samples.

The percentages of the elements were calculated by atomic absorption spectroscopy (AAS) and C, N, H elemental analysis. **1**: $C_{160}H_{48}N_{32}Ni_6O_{62.5}V_{18}$: calcd. C 22.32, H 2.22, Ni 10.91, V 28.39, N 5.20; found C 22.30(2), H 2.20(3), Ni 10.81(2), V 28.32(2), N 5.19(2). **2**: calcd. C 32.62, H 2.27, N 4.21, Ni 8.82, V 30.62; found C 32.60(4), H 2.20(2), N 4.19(2), Ni 8.80(4), V 30.52(4). The density was measured by the flotation method in a mixture of bromoform/cloroform being, 2.12(2) g/cm^{-3} (for **1**) and 2.11(2) g/cm^{-3} (for **2**).

Single-Crystal X-ray Diffraction: Prismatic single-crystals of **1** and **2**, with dimensions given in Table 3, were selected under a polarising microscope and mounted on a glass fibre. Single-crystal X-ray diffraction data were collected at 100 K (for **1**) and 150 K (for **2**) on an STOE IPDS (Imaging Plate Diffraction System) automatic diffractometer (Mo-K_α radiation). Details of crystal data and some features of the structure refinements are reported in Table 3. Lattice constants were obtained by using a standard program belonging to the software of the diffractometer, confirming at the same time the good quality of the single crystal.

The Lorentz polarization and absorption corrections were made with the diffractometer software, taking into account the size and shape of the crystals.[27] The structures were solved by direct methods (SHELXS97).[28] The refinement of the crystal structures was performed by full-matrix least-squares based on F^2, using the SHELX97 program.[29] Scattering factors were taken from ref.[30]

Table 3. Crystal data and structure refinement for **1** and **2**.

Compound	**1**	**2**
Formula	$C_{160}H_{48}N_{32}Ni_6O_{62.5}V_{18}$	$C_{12}H_{14}N_2NiO_{13}V_4$
Fw [g/mol]	3206.28	664.72
Crystal system	monoclinic	monoclinic
Colour	yellow	red
Space group	$P2_1$	$P2_1/c$
a, *b*, *c* [Å]	18.6048(4), 12.4654(3), 21.7505(5)	7.2721(3), 23.062(2), 12.4826(6)
β [°]	91.489(2)	91.245(4)
Z, *F*(000), *T* [K]	2, 3148, 100	4, 1312, 150
μ [mm^{-1}]	2.778	2.675
$\rho_{calcd.}$, $\rho_{obsd.}$ [g cm^3]	2.113, 2.12(2)	2.110, 2.11(2)
Crystal size [mm]	$0.14 \times 0.07 \times 0.03$	$0.2 \times 0.1 \times 0.05$
Radiation (λ) [Å]	0.71073	0.71073
Number of reflections	20443	4588
Reflections with $I > 2\sigma(I)$	18359	2778
h,*k*,*l*	$-23 \geq h \geq 23$, $-15 \geq k \geq 15$, $-27 \geq l \geq 27$	$-8 \geq h \geq 9$, $-29 \geq k \geq 29$, $-15 \geq l \geq 15$
R(int), *R*(sigma)	0.000, 0.0607	0.0546, 0.0938
R_1, wR_2(obsd.) [$I > 2\sigma(I)$]	0.0574, 0.1309	0.0330, 0.0419
R_1, wR_2(all)	0.0681, 0.1381	0.0769, 0.0469
GooF *S*	1.060	0.758
Number of parameters/restraints	1007, 1	306,6
Largest diff. peak [e Å^{-3}]	1.862	–0.828
Largest diff. hole [e Å^{-3}]	–0.960	0.089

The crystal structure of **1** was solved in the monoclinic $P2_1$ space group which allowed to determine the positions of the Ni, V and O atoms. The C and N atoms were located in the difference density map. Anisotropic thermal parameters were used for all atoms except for the H atoms belonging to the organic molecule, which were fixed geometrically and allowed to ride on their parent C atoms (C–H: 0.95 Å), and refined with common isotropic displacements. The H atoms of coordinated water molecules were not located.

At this stage of the refinement some of the oxygen atoms belonging to the vanadate chains show non-positive definite geometries. We performed several attempts to resolve the crystal structure in the centrosymmetric space groups $P2_1/c$, and $P2_1/m$, localizing all the atoms except for the vanadium and oxygen atoms belonging to the V_2O_7 dimers. The crystal structure possesses a strong pseudosymmetry relating the nickel octahedra, VO_5 polyhedra, and the organic molecules, but not the V_2O_7 dimers.[31] Moreover, the systematic absences (*h* 0 *l*) are clearly broken, and the refinement in the centric groups gives rise to unreasonable chemical models. The large correlations between the symmetry related parts of the final crystal structure gives rise to problems in the anisotropic thermal displacements of the atoms belonging to these ones. For these reasons we have used equal anisotropic displacements for the carbon and nitrogen atoms of the organic molecule, and for the tri-coordinated oxygen atoms of the VO_5 polyhedra. The absolute parameter 0.337(13) indicates a racemic twining of both enantiomers. The structure of **2** was solved in the $P2_1/c$ space group. Anisotropic thermal displacements were used for all non hydrogen atoms. Some of the vanadium and oxygen atoms of the vanadium oxide subunit are disordered in two positions with occupation factor 0.5. Equal anisotropic thermal displacements were used for the disordered vanadium atoms, tri-coordinated oxygen atoms, and bi-coordinate and terminal ones. Hydrogen atoms belonging to the organic molecule were located at calculated their positions using a riding model, while the hydrogen atoms of the coordinated water molecules were located in the Fourier density maps and refined with isotropic thermal displacements. The O–H bond length was restrained to 0.93(1) Å. The hydrogen atoms attached to co-crystallized water molecules were not located. Details of crystal data, data measuring and reduction, structure solution and refinement are reported in the Table 3.

CCDC-736371 (for **1**) and -736372 (for **2**) contain the supplementary crystallographic data for this paper. These data can be obtained free of charge from The Cambridge Crystallographic Data Centre via www.ccdc.cam.ac.uk/data_request/cif.

Physical Measurements: The infrared spectra were recorded on a Jasco FT/IR-6100 spectrometer with pressed KBr pellets. The IR spectra were recorded for pristine samples of **1** and **2**, and after heating these ones up to 100, 125, 150, 175, 200, 225 and 250 °C during one hour. Thermal analyses were performed in air atmosphere, up to 500 °C, with a heating rate of 5 °C min^{-1} on a DSC 2960 Simultaneous DSC-TGA TA Instrument. The temperature-dependent PXRD in air atmosphere for 1 was realized on a PHILIPS X'PERT diffractometer (Cu-K_α radiation), equipped with a variable-temperature stage (Paar Physica TCU2000) with Pt sample holder. Patterns were recorded each 10 °C from 30 °C to 800 °C (2θ step: 0.05°, 2θ range: 5–35.2°, time exposure: 1 s per step). The temperature-dependent PXRD in air for **2** was carried on a Bruker Advance Vantec diffractometer (Cu-K_α radiation), equipped with a variable-temperature stage (HTK2000) with Pt sample holder. Patterns were recorded each 10 °C from 30 °C to 500 °C (2θ step: 0.033°, 2θ range: 5–33.0, time exposure: 0.5 s). Diffuse reflectance spectra were registered at room temperature on a Varian Cary 50000 spectrophotometer in the 50000–4000 cm^{-1} range. Magnetic measurements of a powdered sample were performed in the temperature range 5–300 K, using a Quantum Design MPMS-7 SQUID magnetometer. The magnetic field was 0.1 T.

Supporting Information (see also the footnote on the first page of this article): Disorder of the VO_5 polyhedra of the metavanadate chains for **2** (Figure S.1). Bond length histograms for **1** (Figure S.2). Bond lengths for **2** (Figure S.3). TGA and ATD curves (Figure S.4). Thermodiffractometry for **1** and **2** (Figure S.5). Thermal evolution of the (020) and (011) reflections during the transformation, as a result of removal of coordinated water molecules, for **2**. Qualitative model for the transformation due to the loss of coordinated water molecules (Figure S.6, parts a and b, respectively). IR spectra

for the pristine samples of **1** and **2** (Figure S.7). IR spectra for the pristine samples of **1** and heated ones at 125, 150, 175, 200, 225, 250 °C during one hour (Figure S.8). IR spectra for the pristine samples of **1** and heated probes at 125, 150, 175, 200, 225, 250 °C during one hour (Figure S.9). Magnetic exchange pathway for the compound **2** (Figure S.10).

Acknowledgments

Financial support of this work by the Spanish Ministerio de Educación y Ciencia (MEC) (MAT2007-60400/66737-C02-01) and by Gobierno Vasco (IT-177-07 and GI07/126-IT-312-07) is gratefully acknowledged. The authors wish to thank the technicians of SGIker, Drs. J. Sangüesa, I. Orue, P. Vitoria and A. Larrañaga for performing X-ray diffraction and magnetic measurements, respectively. Their work was financed by the Ministerio de Ciencia y Tecnología (MCYT) and Fondo Social Europeo (FSE) (National Program for the Promotion of Human Resources within the National Plan of Scientific Research, Development and Innovation). R. F. d. L. thanks the MEC (BES-2005-10322) for financial support.

[1] a) S. Kitagawa, R. Kitaura, S.-I. Noro, *Angew. Chem. Int. Ed.* **2004**, *43*, 2334–2375; b) U. Mueller, M. Schubert, F. Teich, H. Puetter, K. Schierle-Arndt, J. Pastré, *J. Mater. Chem.* **2006**, *16*, 626–636.
[2] a) P. J. Hargman, D. Hargman, J. Zubieta, *Angew. Chem. Int. Ed.* **1999**, *38*, 2638–2684; b) P. Y. Zavalij, M. S. Whittingham, *Acta Crystallogr., Sect. B* **1999**, *55*, 627–810.
[3] a) W. Li, J. R. Dahn, D. S. Wainwright, *Science* **1994**, *264*, 1115; b) X. Qu, G. Gao, F. Li, Y. Yang, *Inorg. Chem.* **2007**, *46*, 4775; c) M. S. Whittingham, M. Song, S. Lutta, P. Y. Zavalij, N. A. Chernova, *J. Mater. Chem.* **2005**, *15*, 3362.
[4] a) G. Centi, F. Trifiro, *Appl. Catal. A* **1996**, *143*, 3; b) M. I. Khan, S. Tabussum, C. L. Marshall, M. K. Neylon, *Catal. Lett.* **2006**, *112*, 1.
[5] P. A. Maggard, H. Lin, *Inorg. Chem.* **2008**, *47*, 8044.
[6] P. J. Hargman, D. Hargman, J. Zubieta, *Angew. Chem. Int. Ed.* **1999**, *38*, 2638.
[7] V. A. Blatov, L. Carlucci, G. Ciani, D. M. Proserpio, *CrystEngComm* **2004**, *6*, 377.
[8] a) E. S. Larrea, J. L. Mesa, J. L. Pizarro, M. I. Arriortua, T. Rojo, *J. Solid State Chem.* **2007**, *180*, 1149–1157; b) L.-M. Zheng, X. Wang, Y. Wang, A. J. Jacobson, *J. Mater. Chem.* **2001**, *11*, 1100–1105; c) R. L. LaDuca Jr., R. S. Rarig Jr., J. Zubieta, *Inorg. Chem.* **2001**, *40*, 607–612.
[9] a) M. I. Khan, E. Yohannes, R. C. Nome, S. Ayesh, V. O. Golub, C. J. O′Connor, R. J. Doedens, *Chem. Mater.* **2004**, *16*, 5273–5279; b) R. N. Devi, P. Rabu, V. O. Golub, C. J. O'Connor, J. Zubieta, *Solid State Sci.* **2002**, *4*, 1095–1102.
[10] a) L. Yang, C. Hu, H. Naruke, T. Yamase, *Acta Crystallogr., Sect. C* **2001**, *57*, 799–801; b) C.-L. Chen, A. M. Goforth, M. D. Smith, C.-Y. Su, H.-C. zur Loye, *Angew. Chem. Int. Ed.* **2005**, *44*, 6668–6673.
[11] a) T. Chirayil, P. Y. Zavalij, M. S. Whittingham, *Chem. Mater.* **1998**, *10*, 2629–2631; b) L. Bouhedja, M. Steunou, J. Maquet, J. Livage, *J. Solid State Chem.* **2001**, *162*, 315–321.
[12] a) P. A. Maggard, P. D. Boyle, *Inorg. Chem.* **2003**, *42*, 4250–4252; b) B. Yan, J. Luo, P. Dube, A. S. Sefat, J. E. Greedan, P. A. Maggard, *Inorg. Chem.* **2006**, *45*, 5109–5118.
[13] R. Fernández de Luis, M. K. Urtiaga, J. L. Mesa, T. Rojo, M. I. Arriortua, *J. Alloys Compd.* **2008**, *480*, 54–56.
[14] X. Qu, L. Xu, G. Gao, F. Li, Y. Yang, *Inorg. Chem.* **2007**, *46*, 4775–4777.
[15] a) L. Carluci, G. Ciani, D. M. Proserpio, *Coord. Chem. Rev.* **2003**, *246*, 247; b) S. Batten, *CrystEngComm* **2001**, *18*, 1.
[16] a) O. Delgado-Friedrichs, M. O'Keeffe, O. M. Yaghi, *Acta Crystallogr., Sect. A* **2003**, *59*, 22–27; b) O. Delgado-Friedrichs, M. O'Keeffe, *J. Solid State Chem.* **2005**, *178*, 2480–2485; c) http://www.topos.ssu.samara.ru; Blatov, V. A *IUCr CompComm Newsletter* **2006**, *7*, 4–7.
[17] M. Schindler, F. C. Hawthorne, W. H. Baur, *Chem. Mater.* **2000**, *12*, 1248–1259.
[18] a) I. D. Brown, in: *Structure and Bonding in Crystals* (Eds.: M. O'Keeffe, A. Navrotsky), vol. 2, Academic Press, New York, **1981**.
[19] a) H. M. Rietveld, *J. Appl. Crystallogr.* **1969**, *2*, 65–71; b) J. Rodríguez-Carvajal. FULLPROF98, *Program for Rietveld Pattern Matching Analysis of Powder Patterns*, Grenoble, **1998**, unpublished.
[20] E. Baudrin, M. Touboul, G. Nowogrocki, *J. Solid State Chem.* **2000**, *152*, 511–515.
[21] a) M. Calleja, A. L. Goodwin, M. T. Dove, *J. Phys. Condens. Matter* **2008**, *20*, 255226; b) A. L. Goodwin, C. J. Kepert, *Phys. Rev. B* **2005**, *71*, 140301; c) G. D. Barrera, J. A. O. Bruno, T. H. K. Barron, N. L. Allan, *J. Phys. Condens. Matter* **2005**, *17*, R217–R252; d) J. S. O. Evans, *J. Chem. Soc., Dalton Trans.* **1999**, 3317.
[22] a) A. B. P. Lever, *Inorganic Electronic Spectroscopy*, Elsevier Science Publishers B. V., Amsterdam, Netherlands, **1984**; b) T. Y. Sugano, *J. Phys. Soc. Jpn.* **1954**, *9*, 753–766.
[23] K. Nakamoto, *Infrared Spectra of Inorganic and Coordination Compounds*, Wiley, New York, **1986**.
[24] a) R. L. Carlin, *Magnetochemistry*, Springer-Verlag, Berlin, **1986**; b) J. Titiš, R. Boča, L. Dlháň, T. Ďurčeková, H. Fuess, R. Ivaniková, V. Mrázová, B. Papánková, I. Svoboda, *Polyhedron* **2007**, *26*, 1523–1530; c) R. Ivaniková, R. Boča, L. Dlháň, H. Fuess, A. Mašlejová, V. Mrázová, I. Svoboda, J. Titiš, *Polyhedron* **2006**, *25*, 3261–3268.
[25] a) Y. G. Huang, Y. F. Zhou, D.-Q. Yuan, B.-L. Wu, F.-L. Jiang, M.-C. Hong, *J. Mol. Struct.* **2007**, *85*, 830–835; b) M. Kurmoo, H. Kumagai, A. T. Motoko, I. Katsuya, T. Seishi, *Inorg. Chem.* **2006**, *45*, 1627–1637.
[26] R. Fernández de Luis, J. L. Mesa, M. K. Urtiaga, L. Lezama, M. I. Arriortua, T. Rojo, *New J. Chem.* **2008**, *32*, 1582–1589.
[27] C. Katayama, *Acta Crystallogr., Sect. A* **1986**, *42*, 19–23.
[28] G. M. Sheldrick, *SHELXS86, Program for the Solution of Crystal Structures*, University of Göttingen, Germany, **1986**.
[29] G. M. Sheldrick, *SHELXL97, Program for the Refinement of Crystal Structures*, University of Göttingen, Germany **1997**.
[30] W. Yingua, *J. Appl. Crystallogr.* **1987**, *20*, 258–259.
[31] a) D. Watkin, *Acta Crystallogr., Sect. A* **1994**, *50*, 411–437; b) P. Müller, R. Herbst-Irmer, A. L. Speck, T. R. Schneider, M. R. Sawaya, *Crystal Structure Refinement*, Oxford Science Publications, **2006**.

Received: June 18, 2009
Published Online: September 30, 2009

